High-order harmonic generation in relativistic ionization of magnetically dressed atoms

R. E. Wagner, Q. Su, and R. Grobe
Intense Laser Physics Theory Unit and Department of Physics, Illinois State University, Normal, Illinois 61790-4560
(Received 13 April 1999)

We study the generation of high-order harmonics during the ionization process for atoms described by relativistic classical mechanics with a special focus on retardation and Doppler shifts. We will then extend the discussion to a regime for which the atom-laser interaction takes place in a static homogeneous magnetic field. We demonstrate theoretically the possibility to tune the strength of the magnetic field to relativistic resonances to enhance the frequency components in the scattered light harmonic signal. [S1050-2947(99)00810-0]

PACS number(s): 42.65.Ky, 32.80.Fb

I. INTRODUCTION

It is well known that the ionization of atoms and molecules in strong laser fields can be accompanied by the emission of radiation of very high frequency [1]. For example, experiments by Zhou *et al.* [2] have demonstrated the generation of coherent radiation with a photon energy of 310 eV, corresponding to the 211th harmonic of the laser fundamental frequency [3–5].

The frequency spectrum of the scattered light has been generally characterized by a long plateau associated with odd multiples of the fundamental frequency of the laser and a relatively rapid cutoff. It has been predicted that the harmonics are created during those moments of the interaction where the ionized electron rescatters from the nucleus [6–8]. This led to the so-called $3U_p$ rule and has been confirmed by quantum-mechanical calculations. In most investigations, the maximum frequency increases with the laser intensity. However, if the intensity is too large, the atom ionizes and the nucleus becomes irrelevant for the electron and the maximum harmonic order drops significantly because of the lack of a rescattering center. The atomic stabilization phenomenon (suppression of ionization) [9] certainly increases the maximum harmonic order, but the magnetic-field component of the laser, which leads to an irreversible and unavoidable drift away from the nucleus, can reduce the effect of stabilization.

Originally, theoretical investigations examined only the spectra of single atoms. The details of the propagation of the generated harmonics through the gas jet were neglected. Only in the past five years have theoretical studies been conducted on the propagation effects [10–12] resulting in the investigation of the intensity-dependent phase relationship [13–15] between the fundamental and the harmonic field. Semiclassical studies have shown that the phase of the induced dipole is quite universally a piecewise linear function of the intensity [16]. It is now believed that propagation effects are essential to explain the basic features of the experimentally observed spectra. In this paper we examine the spectra of single atoms; work that incorporates propagation will be devoted to future studies. Our intention is not to produce quantitatively accurate experimental spectra, but to obtain first insights into the novel relativistic dynamics of atoms in strong magnetic fields.

In 1993, Keitel, Knight, and Burnett [17] investigated the generation of higher harmonics for laser intensities that are so strong that a relativistic description of the atom-laser interaction was required. They modeled the quantum state with a classical ensemble and found that the numerical spectra for the dynamics with and without the atomic binding potential were very similar. This suggests that most of the harmonics were due to the relativistic orbit of a free electron and not due to its interaction with the nucleus.

In this paper we will investigate whether it is possible to increase the efficiency of high-order harmonic generation in the relativistic regime by adding a homogeneous magnetic field to the interaction. Despite the very large number of works that investigate higher harmonics, we are aware of only three studies that examined the scattered light spectra in the presence of magnetic fields. Using a classical ensemble calculation, Connerade and Keitel [18] showed numerically for the case of a magnetic field that is parallel to the laser's polarization direction that the scattered light spectrum also features even harmonics. Zuo *et al.* [19] have applied a single magnetic field in parallel to a two-color laser field that ionizes the electron from the molecular ion H_2^+. Their quantum-mechanical calculations suggested that the transverse magnetic confinement of the electron's wave packet reduces the spreading and enhances the high-order harmonic generation efficiency. Very recently, Milosevic and Starace [20] used classical orbit calculations based on the recollision model for the magnetic-field case and found field-induced intensity revivals in the spectra.

The paper is organized as follows. In Sec. II we describe our model system and derive three expressions for numerical computations of the scattered light spectra using the Lienard-Wiechert potential. These expressions are used in Secs. III and IV. In Sec. III we show how the spectra change from the weak field to the relativistic regime. In the relativistic regime we present analytical formulas for the spectra and compare them with numerical results. In Sec. IV we demonstrate how the individual regimes discussed in Sec. III are modified by an additional magnetic field and propose a simple model to explain some of the spectral features. We also show how the relativistic resonances can be exploited to enhance the higher frequencies in the spectra. We conclude with a discussion and an outline of future work.

II. THE MODEL SYSTEM AND THE SCATTERED LIGHT SPECTRA

The relativistic interaction of a classical electron with an external laser field and a static magnetic field in the presence of an atomic binding potential is described by the square-root Klein-Gordon Hamilton function:

$$H=\{c^4+c^2[\mathbf{p}+\mathbf{A}(\mathbf{r},t)/c]^2\}^{1/2}+V(r). \tag{2.1}$$

We have chosen atomic units and the screened Coulomb potential $V(r)=-1/\sqrt{[r^2+1]}$ in our simulations. It has been demonstrated [21] that predictions of classical trajectories associated with this screened potential approximate the quantum-mechanical calculations for the $-1/r$ potential much closer than those obtained classically with the singular $-1/r$ potential binding. The vector potential $\mathbf{A}(\mathbf{r},t)$ in Eq. (2.1) is the sum of two parts, one modeling the external laser field linearly polarized along the x direction with electric-field amplitude E_0. The other part corresponds to a static homogeneous magnetic field of strength B_z along the z direction:

$$\mathbf{A}(\mathbf{r},t)=(c/\omega_L)E_0 f(t-y/c)\sin(\omega_L t-ky)\mathbf{e}_x+\tfrac{1}{2}\mathbf{r}\times(B_z\mathbf{e}_z), \tag{2.2}$$

where ω_L denotes the laser frequency, k is the wave number, and $\mathbf{e}_x$ and $\mathbf{e}_z$ are the Cartesian unit vectors. The pulse envelope function $f(\,)$ is chosen with a trapezoidal shape, which is linearly turned on and off for two optical cycles and has a constant amplitude for 30 optical cycles. The laser frequency was chosen to be $\omega_L=0.15$ a.u. The total interaction time in most calculations was $34\times 2\pi/\omega_L=1424.19$ a.u. (34 fs).

The trajectories were solved in canonical variables using a Runge-Kutta fourth-order algorithm with self-adapting step size. This algorithm is very accurate and reliable, which is necessary if very-high-frequency components of the orbits need to be resolved.

For nonrelativistic field strengths, the spectrum of the scattered light can be computed directly via the Fourier transformation of the time-dependent position, velocity, or acceleration of the electron. However, the Doppler shift, time contraction, and retardation effects can be important in the relativistic regime and the spectrum must be calculated from the solution of the wave equation for the vector potential [22]. The scattered electric field depends on the (normalized) observation direction $\mathbf{n}$ and the distance $R=|\mathbf{d}-\mathbf{r}|$ between the detector located at $\mathbf{d}$ and the electron located at $\mathbf{r}$. The radiation (far-field) part of the Lienard-Wiechert electric field $\mathbf{E}$ has the well-known form

$$\mathbf{E}(t)=\frac{1}{c}\mathbf{n}\times\{[\mathbf{n}-\boldsymbol{\beta}(t_r)]\times\dot{\boldsymbol{\beta}}(t_r)/[1-\mathbf{n}\cdot\boldsymbol{\beta}(t_r)]^3\}/R(t_r), \tag{2.3}$$

where t_r denotes the retarded time defined via the implicit relation $t_r\equiv t-R(t_r)/c$ and the (scaled) electron velocity $\boldsymbol{\beta}\equiv\mathbf{v}/c$. Due to the implicit definition of the retarded time, the electron trajectory needs to be inverted numerically to compute the scattered electric field at the detector in laboratory time t [17]. In our case we are not interested in the time dependence of the scattered field but rather in its Fourier spectrum, and this cumbersome inversion can be avoided. The energy radiated per unit solid angle per unit frequency at the detector is defined via

$$\begin{aligned}\mathbf{I}_\mathbf{n}(\omega)&=(c/4\pi^2)\left|\int_{-\infty}^{\infty}dt\,\exp(i\omega t)R(t_r)\mathbf{E}(t_r)\right|^2\\&=(1/4\pi^2 c)\left|\int_{-\infty}^{\infty}dt\,\exp(i\omega t)\mathbf{n}\times\{[\mathbf{n}-\boldsymbol{\beta}(t_r)]\right.\\&\left.\times\dot{\boldsymbol{\beta}}(t_r)\}/[1-\mathbf{n}\cdot\boldsymbol{\beta}(t_r)]^3\right|^2.\end{aligned} \tag{2.4}$$

For the special case that the laser is so weak such that the velocities are nonrelativistic ($\beta\ll 1$), we can neglect retardation ($t_r\approx t$) and the spectrum can be computed directly from the Fourier transformation of the acceleration, or equivalently, the position (dipole moment). Switching the integration variable t to the retarded time, via $t=t_r+R(t_r)/c$, and assuming that the detector is far away from the electron, such that $R(t_r)\approx d-\mathbf{n}\cdot\mathbf{r}(t_r)$, where d is the distance from the atom to the detector, we obtain the expression

$$\begin{aligned}\mathbf{I}_\mathbf{n}(\omega)&=(c/4\pi^2)\left|\int_{-\infty}^{\infty}dt_r[1-\mathbf{n}\cdot\boldsymbol{\beta}(t_r)]\right.\\&\left.\times\exp[i\omega t_r-i\omega\mathbf{n}\cdot\mathbf{r}(t_r)/c]R(t_r)\mathbf{E}(t_r)\right|^2.\end{aligned} \tag{2.5}$$

For the case in which the motion of more than one electron is involved, the vector contributions of the integrand have to be summed up. The specific form of $\mathbf{E}(t_r)$ from Eq. (2.3) can be inserted into Eq. (2.5) and integrated by parts using the identity $\mathbf{n}\times[(\mathbf{n}-\boldsymbol{\beta})\times\dot{\boldsymbol{\beta}}]/(1-\mathbf{n}\cdot\boldsymbol{\beta})^2=(d/dt)\mathbf{n}\times(\mathbf{n}\times\boldsymbol{\beta})/(1-\mathbf{n}\cdot\boldsymbol{\beta})$. We obtain a much simpler expression,

$$\begin{aligned}\mathbf{I}_\mathbf{n}(\omega)&=\omega^2/(4\pi^2 c)\left|\int_{-\infty}^{\infty}dt\,\mathbf{n}\times(\mathbf{n}\times\boldsymbol{\beta})\right.\\&\left.\times\exp\{i\omega[t-\mathbf{n}\cdot\mathbf{r}(t)/c]\}\right|^2.\end{aligned} \tag{2.6}$$

Note that in expression (2.6) we have omitted the subscript r from the integration variable, and the cumbersome inversion mentioned above has been avoided.

In the text below we will refer to $I_x(\omega)$ as the spectrum observed in the polarization direction, $I_y(\omega)$ in the forward (propagation) direction of the pulse, and $I_z(\omega)$ as the scattered fields emitted parallel to the magnetic-field component of the laser field. To accurately describe the high-frequency components in the spectrum, the orbit was monitored for 32 768 points, which is only a very small fraction of the actual integration steps used in the calculation. We have computed the scattered light spectra via three different methods: the spectrum was first calculated from Eq. (2.4) and the implicit relation $t_r\equiv t-R(t_r)/c$ was solved numerically for t_r for each time step t required by the integration. The spectra agreed precisely with those computed via the integrals of Eq. (2.5) and also Eq. (2.6). The spectra due to Eqs. (2.5) and

(2.6), however, take more CPU time because the convenient fast Fourier transformation (FFT) routines cannot be used in evaluating the integrals.

III. HIGH-ORDER HARMONIC SPECTRA IN THE ABSENCE OF THE MAGNETIC FIELD

In order to get a more systematic understanding of the full complexity of the scattered light spectra, we have scanned the laser intensity and found that there are three distinct regimes of interaction, which we review in this section. In Sec. IV we will show how these regimes are modified due to the magnetic field.

A. Weak electric-field regime

We have monitored the spectra obtained from a trajectory bound at $\mathbf{r}=\mathbf{0}$ initially and with velocity $\dot{\mathbf{r}}=(0.1,0,0)$. The electron was evolved for a time of 3000 a.u. in the absence of any external laser field, $E_0=0$. The resulting spectra $I_y(\omega)$ and $I_z(\omega)$ (not shown) contain a peak at the ''bare atomic'' frequency of $\omega_b=0.995$ a.u. and a rapidly falling-off sequence of its odd-order multiples at $(2n+1)\omega_b$ [23,24]. The value for the atomic frequency ω_b can also be obtained easily by using the energy conservation and integrating numerically $dt=dx/\sqrt{\{2[E-V(x)]\}}$ over one atomic period, where E denotes the energy as given by the initial condition ($E \equiv \dot{\mathbf{r}}^2/2-1$ in this case).

We have repeated our simulation but subjected the atom to 34 cycles of a laser field with amplitude $E_0=0.16$ a.u. We chose a square pulse here to have narrower peaks that allow for a higher resolution due to the absence of additional peaks typically associated with a pulsed laser field. The laser frequency was $\omega_L=0.15$ a.u. as in all of our simulations.

In the top of Fig. 1 we display the spectrum $I_z(\omega)$. The dominant peak corresponding to the atomic frequency is slightly redshifted by $\Delta\omega=0.051$ a.u. to $\omega=0.944$ a.u., which we define here as the (field-dressed) atomic frequency ω_a. Each peak in the spectrum can be easily associated with a certain linear combination of the laser frequency ω_L and the (dressed) atomic frequency ω_a according to $\omega(L,M)\equiv L\omega_L + M\omega_a$, where $L,M=0,\pm1,\pm2,\pm3,\ldots$. We have marked the locations of these distinct frequencies $\omega(L,M)$ in the figure by the dashed vertical lines and labeled them according to the two integers L and M. It is interesting to note that only frequencies for which the sum $L+M$ is an odd integer have appreciable amplitudes. The absence of any even harmonics ($L+M=$even) is due to the inversion symmetry of the Coulomb potential. This result is expected and can be easily shown perturbatively for small displacements if one uses the fact that the Taylor expansion of the binding force contains only odd powers of the position coordinates.

B. Strong electric-field regime

In the middle of Fig. 1 we display the spectrum for the laser field strength $E_0=0.331$ a.u., which is slightly below the ionization threshold for this particular trajectory. For this field strength the laser harmonics are comparable or even stronger than those associated with the atomic frequency, which has been redshifted to $\omega_a\approx0.8$ a.u. The spectrum is clearly dominated by peaks associated with the series $(L,0)$

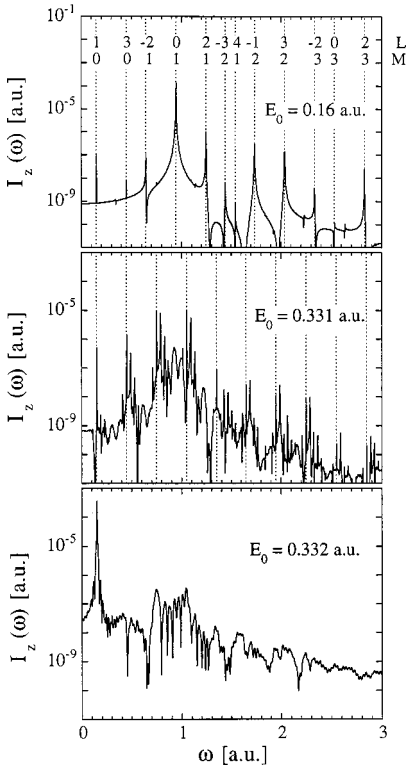

FIG. 1. Nonrelativistic scattered light spectra $I_z(\omega)$ without the magnetic field. Scattered light spectrum in the laser field with frequency $\omega_L=0.15$ a.u. for three values of the electric-field amplitude E_0. The dashed lines in (a) are labeled with the integers (L,M) corresponding to the predicted location of the peaks as in $(L\omega_L + M\omega_a)$ using the dressed atomic frequency $\omega_a=0.944$ a.u. The corresponding spectra are very similar in the y-observation direction. The electron had the initial conditions $\mathbf{r}(0)=(0.1,0,0)$ and $\dot{\mathbf{r}}(0)=0$. (Top) $E_0=0.16$ a.u. (mainly bound dynamics) (34-cycle square pulse). (Middle) $E_0=0.331$ a.u. (slightly below ionization) (trapezoidal pulse of length 34 cycles with two cycle turn-on and off). (Bottom) $E_0=0.332$ a.u. (slightly above ionization, same pulse shape as for $E_0=0.331$ a.u.).

as shown by the dashed lines and $(L,1)$. In each case the maximum integer L is about 29 or 30. This (possibly accidentally) agrees with the cutoff frequency as predicted by the $3-U_p$ rule according to $0.5+3.2(E_0/2\omega_L)^2\approx29\times0.15$ a.u. In this highly nonperturbative regime, the force due to the laser (0.33 a.u.) is comparable to that of the nucleus (0.38 a.u.) so that neither the laser nor the Coulomb field can be regarded as a small perturbation. As a consequence, the efficiency of higher harmonic generation becomes maximum.

In the bottom of Fig. 1 we show the spectrum corresponding to a laser field strength $E_0=0.332$ a.u., which is above the ionization limit for this trajectory. The spectrum is drastically different and only the fundamental laser frequency is present. Its intensity $I_z(\omega_L)$ is three orders of magnitude larger than for $E_0=0.331$ a.u. The electron has ionized quickly and cannot rescatter with the nucleus to generate the higher frequencies. The abrupt transition between the spectra clearly shows the importance of the atomic potential with respect to the efficiency of higher-harmonics generation in the nonrelativistic regime. If we could prohibit ionization we would expect the generation of much higher harmonics for larger

laser fields. In Sec. IV we will show how suitable magnetic fields may be used to achieve this.

We should mention that for the (nonrelativistic) regime displayed in Fig. 1, the spectra are dominated by the electron's orbit along the x direction and are therefore practically identical in the y and z observation direction: $I_y(\omega) \approx I_z(\omega)$. The spectrum $I_x(\omega)$ is several orders of magnitude smaller because a nonrelativistic dipole does not radiate along its direction of motion.

C. Relativistic electric-field regime

As the atom becomes rapidly ionized in the relativistic region, one would expect that the spectral response of the atom to the field is similar to that of a free electron in the absence of the binding potential [17]. For this case one can derive analytically the scattered light spectra for the electron. In 1955, Landau and Lifshitz [25] have shown that the solutions to the relativistic equations of motion for a free electron in laboratory time $\mathbf{r}(t)$ have to satisfy the transcendental equations

$$x(t)=\frac{E_0}{\omega_L^2}(\cos\omega_L\tau-1)\equiv\tilde{x}(\tau), \tag{3.1a}$$

$$y(t)=\frac{E_0^2}{4\omega_L^2 c}\tau-\frac{E_0^2}{8\omega_L^3 c}\sin 2\omega_L\tau\equiv\tilde{y}(\tau), \tag{3.1b}$$

$$z(t)=0\equiv\tilde{z}(\tau), \tag{3.1c}$$

where we have chosen $\mathbf{r}(0)=\dot{\mathbf{r}}(0)=0$ for convenience, corresponding to an electron at rest at the origin before the laser field is turned on. It turns out that the parameter $\tau\equiv t-y(t)/c$ is also the electron's local time [26,27]. Equations (3.1) describe the well-known drifting ''figure-eight'' motion in the $[\tilde{x}(\tau),\tilde{y}(\tau)]$ plane as a function of the parameter τ [28]. Unfortunately, this simple trajectory is less apparent for an observer in the laboratory frame recording the emitted harmonic signals. To inspect the ''real'' motion of the electron in the laboratory time and laboratory coordinates, we solve these equations iteratively and taking only the leading orders in $1/c$ we obtain

$$x(t)=\frac{E_0}{\omega_L^2}\left\{\cos\left[(1-\alpha)\omega_L t+\frac{\alpha}{2}\sin(2\omega_L t)\right]-1\right\}, \tag{3.2a}$$

$$y(t)=\alpha c t-\frac{\alpha c}{2\omega_L}\sin[2(1-\alpha)\omega_L t-\alpha\sin(\omega_L t)]. \tag{3.2b}$$

Here we have defined the dimensionless parameter $\alpha\equiv E_0^2/(E_0^2+4\omega_L^2c^2)$, which can be viewed as a measure for the ratio of the ponderomotive energy $(E_0/2\omega)^2$ to the electron's total energy. The redshifted frequency $(1-\alpha)\omega_L$ has an immediate interpretation: Due to the magnetic-field component of the laser, the electron drifts with an average speed αc in the y direction and therefore experiences a Doppler-shifted laser frequency ω_L^D in its own rest frame: $\omega_L^D=\omega_L\sqrt{(1-\alpha)/(1+\alpha)}$. By Lorentz-transforming this frequency ω_L^D back to the laboratory time, we obtain $\omega_L^D\sqrt{1-\alpha^2}=(1-\alpha)\omega_L$, which is precisely the same value as derived perturbatively from Eq. (3.2).

We should comment that the leading correction to the nonlinear relativistic response of the electron is due to the nonlinear driving force proportional to $\sin[\omega_L(t-y/c)]$, associated with the magnetic-field component of the laser. The kinematic relativistic effects, such as a nonlinear mass increase, enter the solutions only for higher orders of α.

It is quite remarkable that even though the electron's motion in the laboratory frame is not known analytically without the iterative procedure outlined above, the frequency spectrum of the scattered light can be calculated fully analytically. The basic trick to solve the required integral of Eq. (2.5) is to change the integration variable to the electron's local time τ, for which the expressions in Eqs. (3.1) can be used [29–31]:

$$\mathbf{I}_\mathbf{n}(\omega)=(\omega^2/4\pi^2c)\left|\int_{-\infty}^{\infty}d\tau\,\mathbf{n}\times(\mathbf{n}\times\boldsymbol{\beta})\exp\{i\omega[\tau+\tilde{y}(\tau)/c-\mathbf{n}\cdot\tilde{\mathbf{r}}(\tau)/c]\}\right|^2. \tag{3.3}$$

Using the Bessel-Anger expansion for the trigonometric functions in the exponent, the integrals can be solved fully analytically and we obtain the spectra for the three observation directions:

$$I_x(\omega)=\sum_{m=0}^{\infty}A_x(m)\,\delta^2(\omega-(2m+1)(1-\alpha)\omega_L)+\sum_{m=0}^{\infty}B_x(m)\,\delta^2(\omega-2m(1-\alpha)\omega_L), \tag{3.4a}$$

$$I_y(\omega)=(E_0\omega)^2/(4c^3\omega_L^2)\,\delta^2(\omega-\omega_L), \tag{3.4b}$$

$$I_z(\omega)=\sum_{m=0}^{\infty}A_z(m)\,\delta^2(\omega-(2m+1)(1-\alpha)\omega_L)+\sum_{m=0}^{\infty}B_z(m)\,\delta^2(\omega-2m(1-\alpha)\omega_L), \tag{3.4c}$$

where the amplitudes for the odd- and even-order harmonics are given in terms of the ordinary Bessel functions of the first kind with integer order:

$$A_x(m)\equiv[(\alpha\omega)^2/c]\left\{\sum_{k=0}^{\infty}(-1)^k\{[1-2(m+k+1)(1-\alpha)\times\omega_L/(\alpha\omega)]J_{m+k+1}(\alpha\omega/[2(1-\alpha)\omega_L])+[1-2(m-k)(1-\alpha)\omega_L/(\alpha\omega)]\times J_{m-k}(\alpha\omega/[2(1-\alpha)\omega_L])\}\,J_{2k+1}(\omega E_0/(c\omega_L^2))\right\}^2, \tag{3.4d}$$

$$B_x(m)\equiv[(\alpha\omega)^2/c]\left\{[1-2m(1-\alpha)\omega_L/(\alpha\omega)]\times J_m(\alpha\omega/[2(1-\alpha)\omega_L])J_0(\omega E_0/(c\omega_L^2))+\sum_{k=1}^{\infty}(-1)^k([1-2(m+k)(1-\alpha)\omega_L/(\alpha\omega)]\right.$$

$$\times J_{m+k}(\alpha\omega/[2(1-\alpha)\omega_L]) + [1-2(m-k)(1-\alpha)\omega_L/(\alpha\omega)] \times J_{m-k}\{\alpha\omega/[2(1-\alpha)\omega_L]\})\times J_{2k}[\omega E_0/(c\omega_L^2)]\Big\}^2, \tag{3.4e}$$

$$A_z(m)\equiv(1-\alpha)^2(E_0\omega)^2/(4c^3\omega_L^2) \times\{J_{m+1}(\alpha\omega/[2(1-\alpha)\omega_L]) - J_m(\alpha\omega/[2(1-\alpha)\omega_L])\}^2 \tag{3.4f}$$

$$B_z(m)\equiv 1/c\{[\alpha\omega-2m(1-\alpha)\omega_L]J_m(\alpha\omega/[2(1-\alpha)\omega_L])\}^2. \tag{3.4g}$$

In the above we have used the symbol $\delta^2(x)$ as a shorthand notation for the square of the integral $\int_{-\infty}^{\infty}dt\,\exp(ixt)/2\pi$. In order to allow for a fair comparison with the results of simulations for finite laser pulses of duration T, we have to replace $\delta^2(x)$ in Eqs. (3.4) with scaled sinc functions $\delta^2(x)=\sin^2(xT/2)/(\pi x)^2$. However, we must note that this approximation is only valid if the spacings between the peaks (equal to the redshifted laser frequency) are larger than the inverse pulse duration: $(1-\alpha)\omega_L \gg 2\pi/T$.

The large drift term in $y(t)$ in Eq. (3.2b) suggests that retardation has the largest impact in the positive y direction ($\mathbf{n}=\mathbf{e}_y$). The corresponding scattered light $I_y(\omega)$ contains only the (unshifted) fundamental laser frequency ω_L. Although the electron oscillates with multiples of the (redshifted) frequency $(1-\alpha)\omega_L$, the effect due to retardation exactly cancels this shift as well as the harmonics such that the spectrum contains only the single frequency ω_L.

It should be noted that the spectra $I_{x,z}(\omega)$ contain even and odd harmonics of the redshifted frequency $(1-\alpha)\omega_L$. For smaller laser field strengths, one finds that the amplitude associated with $(1-\alpha)\omega_L$ in the spectrum $I_x(\omega)$ can be smaller than that of the second-harmonic peak at $2(1-\alpha)\omega_L$. The two different forms for the amplitudes associated with the even- and odd-order harmonics suggest a different intensity dependence of these types of harmonics. If the electric-field strength (or the frequency) is so large that the dimensionless parameter $\alpha\omega/[2(1-\alpha)\omega_L]$ exceeds unity and matches a zero of a Bessel function, then the corresponding harmonics could be suppressed.

In Fig. 2 we compare the scattered light spectrum obtained numerically from the electron trajectory with the binding potential with the analytical predictions for a free electron according to Eq. (3.4). The good agreement between the analytical formula for a free electron and that for the ionized electron clearly shows that the observed harmonics are mainly due to the relativistic interaction with the field (and not with the potential). After the pulse, the electron has drifted by more than 37 367 a.u. along the y direction. For the test case of $V(\mathbf{r})=0$, the numerical and analytical curves in each case were completely indistinguishable and the precise peak amplitudes obtained by both methods differed by less than 10^{-3}% up to the 21st harmonic. This demonstrates nicely the reliability and accuracy of the fourth-order Runge-Kutta integration method with adaptive step size.

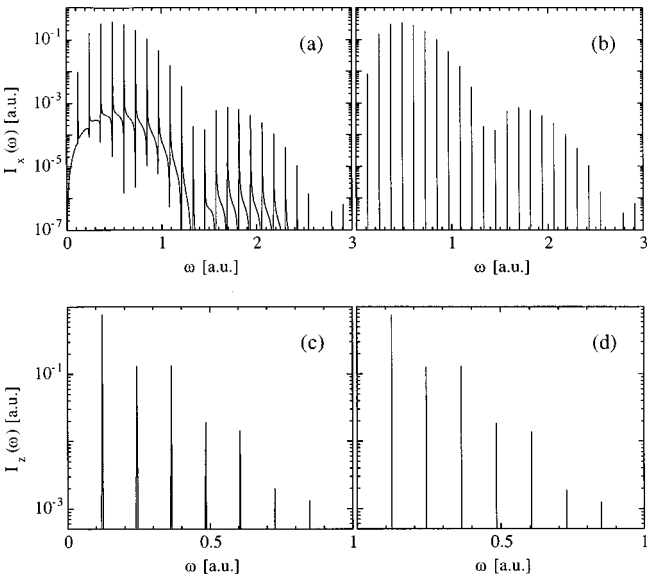

FIG. 2. Relativistic scattered light spectra without the magnetic field. Scattered light spectrum of an (initially bound) trajectory in the laser field with frequency $\omega_L=0.15$ a.u. for the electric-field amplitude $E_0=20$ a.u. detected along the x direction (a),(b) and the z direction (c),(d). The graphs in (b) and (d) show the corresponding analytical predictions according to Eqs. (3.4), based on the free-electron dynamics for a 34-cycle square pulse. Same electron initial conditions as in Fig. 1.

The data shown correspond to a laser field strength $E_0=20$ a.u. associated with $E_0/\omega\approx c$ and $\alpha=0.19$, which shifts the observed fundamental frequency by 79% towards red (to $\omega=0.12$ a.u.). This redshift becomes especially significant for the higher harmonics. The $(n+1)$st harmonic with $n\approx 1/\alpha-1$ has the same frequency as the nth harmonic of the (unshifted) fundamental. For our parameters this would be at $n\approx 4$.

IV. HIGH-ORDER HARMONICS SPECTRA IN THE PRESENCE OF THE MAGNETIC FIELD

We will now investigate how the ionization dynamics and the spectra discussed in Sec. III are affected by the presence of a static magnetic field in the z direction [32].

A. Weak electric-field regime

We begin our analysis by repeating the simulation leading to the top of Fig. 1 but with a static B field of cyclotron frequency $\Omega\equiv B_z/c=0.2$ a.u. Figure 3 shows the spectrum in the direction parallel to the magnetic field $I_z(\omega)$. Unlike the magnetic-field-free case, the spectra for the x and y direction are very similar. Compared to the spectra for $B_z=0$, each peak has split into two and the spectrum looks more complicated. The vertical dashed lines in the figure indicate the predicted peak positions according to a simple perturbative argument and are associated with a set of three integers.

We assume that the laser electric field E_0 is weak enough such that the electron experiences the Coulombic force only in the close vicinity around the nucleus. Thus we can replace the atomic binding potential by a simple harmonic oscillator.

We also assume the dipole approximation. The model Hamilton function for the electron in the combined laser, magnetic, and atomic field in the nonrelativistic limit is described by

$$H=\frac{1}{2}\left[\mathbf{p}+\frac{1}{2c}\mathbf{r}\times B_z\mathbf{e}_z+\frac{E_0}{\omega_L}\sin\omega_L t\hat{\mathbf{e}}_x\right]^2+\frac{1}{2}\omega_a^2\mathbf{r}^2. \quad (4.1)$$

The corresponding equations of motion can be solved analytically. The notation can be simplified if we assume $\mathbf{r}(0)=\dot{\mathbf{r}}(0)=0$, focusing only on the relevant inhomogeneous solution [33],

$$x(t)=\frac{E_0}{\Omega^2\omega_L^2-(\omega_a^2-\omega_L^2)^2}\times\left(\frac{\Omega^2\omega_L^2+(\omega_a^2-\omega_L^2)(\omega_+^2-\omega_a^2)}{\omega_+^2-\omega_-^2}\cos(\omega_- t)-\frac{\Omega^2\omega_L^2+(\omega_a^2-\omega_L^2)(\omega_-^2-\omega_a^2)}{\omega_+^2-\omega_-^2}\cos(\omega_+ t)-(\omega_a^2-\omega_L^2)\cos(\omega_L t)\right), \quad (4.2a)$$

$$y(t)=\frac{E_0/\Omega\omega_a^2}{\Omega^2\omega_L^2-(\omega_a^2-\omega_L^2)^2}\left(\frac{\omega_-(\omega_-^2-\omega_a^2-\Omega^2)[\Omega^2\omega_L^2+(\omega_a^2-\omega_L^2)(\omega_+^2-\omega_a^2)]}{\omega_+^2-\omega_-^2}\sin(\omega_- t)-\frac{\omega_+(\omega_+^2-\omega_a^2-\Omega^2)[\Omega^2\omega_L^2+(\omega_a^2-\omega_L^2)(\omega_-^2-\omega_a^2)]}{\omega_+^2-\omega_-^2}\sin(\omega_+ t)-\omega_L(\omega_L^2-\omega_a^2-\Omega^2)(\omega_a^2-\omega_L^2)\sin(\omega_L t)\right)+\frac{\omega_L E_0}{\Omega\omega_a^2}\sin(\omega_L t). \quad (4.2b)$$

The two frequencies $\omega_\pm(\Omega,\omega_a)$ can be thought of as the magnetically dressed atomic frequencies. They are defined as

$$\omega_\pm(\Omega,\omega_a)\equiv\left[\left(\frac{\Omega}{2}\right)^2+\omega_a^2\right]^{1/2}\pm\frac{\Omega}{2}. \quad (4.3)$$

The magnetic field splits the atomic frequency in two, each of which can be excited independently by the laser. It should be noted that the overall amplitude of the solution reveals the possibility of resonances at $\omega_L=\omega_\pm(\Omega,\omega_a)$. To excite this type of magnetically dressed atomic resonance frequency requires an extremely large magnetic-field strength of the order $B_z=c(\omega_a^2-\omega_L^2)/\omega_L$. The resulting two-dimensional orbits can be complicated, as the three relevant frequencies ω_+, ω_-, and ω_L are generally not commensurate. In the next section we will see that the latter resonance can lead to interesting spectral properties such as an enhancement of even and odd harmonics.

If the laser field is increased, the electron's orbit gets larger and it can also experience the nonlinearity of the atomic potential. A simple perturbative estimate based on the inversion symmetry of the atomic binding potential indicates that the nonlinear (but nonrelativistic) response of the electron is characterized by the following frequencies:

$$\omega(L,M,N)=L\omega_L+M\omega_+(\Omega,\omega_a)+N\omega_-(\Omega,\omega_a), \quad (4.4)$$

where the sum of the three integers $L+M+N$ must be an odd number. This formula led to the dashed lines in Fig. 3.

B. Strong electric-field regime

Due to the presence of the strong magnetic field, the definition of ionization as an irreversible decay of the electron to infinity must be revisited. As is well known from the nonrelativistic limit, a static magnetic field forces the ionized electron into a quasicircular spiral orbit in the plane perpendicular to the magnetic field and the electron can escape irreversibly only along the z direction. In other words, an escape is mainly possible perpendicular to the laser's polarization direction, which is typically the dominant ejection direction for the electrons.

In Fig. 4 we show the ionization spectrum $I_y(\omega)$ for the $E_0=2$ a.u. and a B field (with the ''scaled'' strength) $\Omega=B_z/c=0.4$ a.u. We see the strong peaks at $\omega=\omega_L$ and $\omega=\Omega$ as expected, but also a variety of other peaks. The circles superimposed on the graphs represent the predictions of a simple model that is based on the trajectory of a free electron in a static magnetic field, neglecting those kinematic relativistic effects that govern the evolution of trajectories but including all retardation effects. This model is helpful to

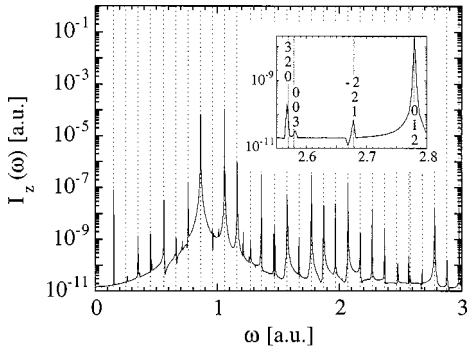

FIG. 3. Nonrelativistic scattered light spectra $I_z(\omega)$. Scattered light spectrum in the laser field with frequency $\omega_L=0.15$ a.u. for the electric-field amplitude $E_0=0.16$ a.u. and static magnetic field with $\Omega=0.2$ a.u. The dashed lines correspond to the location of the peaks as predicted by Eq. (4.4) using the dressed atomic frequency $\omega_a=0.954$ a.u. The inset shows the enlarged spectrum together with the labels (L,M,N) for each peak. The corresponding spectra are very similar to those in the y-observation direction.

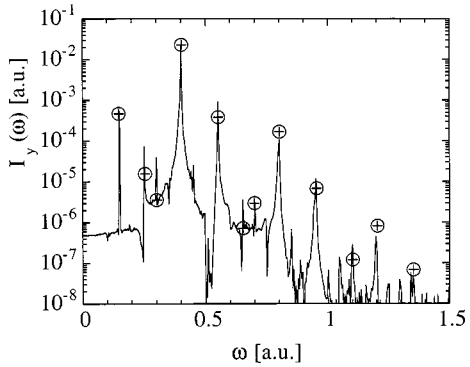

FIG. 4. Predictions of $I_y(\omega)$ for the analytically soluble model. Scattered light spectrum in the laser field for $\omega_L=0.15$ a.u., $E_0=2$ a.u., and $\Omega=0.4$ a.u. The circles are the analytical predictions for the intensity and location of the peaks according to Eq. (4.6), based on the free-electron dynamics in a strong static magnetic field. The laser pulse was a square pulse with 34 optical cycles.

distinguish those spectral aspects that are associated with retardation effects and those that are due to the relativistic nature of the orbits.

In order to derive this model, we can take the solution $x(t)$ and $y(t)$ of Eq. (4.2) for $\omega_a=0$,

$$x(t)=\frac{E_0}{\Omega^2-\omega_L^2}[\cos\omega_L t-\cos\Omega t], \tag{4.5a}$$

$$y(t)=\frac{E_0}{\Omega^2-\omega_L^2}\left(\frac{\Omega}{\omega_L}\sin\omega_L t-\sin\Omega t\right), \tag{4.5b}$$

and use them to calculate the final scattered light spectra according to the Lienard-Wiechert formula (2.6). Unfortunately we have not been able to identify a suitable fully analytical solution for a relativistic electron in a magnetic field driven by a laser field [34]. The omission of kinetic relativistic effects and the dipole approximation in the laser field in Eq. (4.1) are only justified for a certain parameter ranges. If the ''radius'' $E_0/(\Omega^2-\omega_L^2)$ of the electron in the x direction is larger than the laser's wavelength, the dipole approximation breaks down, leading to an upper limit of the laser amplitude: $E_0 \ll \pi c(\Omega^2-\omega_L^2)/\omega_L$. The approximation to neglect relativistic kinematic effects breaks down if the maximum electron velocity approaches the speed of light c, restricting the amplitude according to $E_0 \ll c|\Omega-\omega_L|$. For the special case of the resonance $\Omega=\omega_L$, the latter requirement also restricts the time: after a time $t\approx 2c/E_0$ the electron's velocity would reach c.

The homogeneous solution of Eq. (4.1) (simple circular orbit), which we have omitted here, would lead to the classical synchrotron motion that was first derived by Schott [35,36], who also obtained the total energy loss, polarization, and relativistic contraction. The corresponding spectral distribution was investigated by Schwinger [37]. In our case the laser driven part of the motion is more important than the synchrotron orbit and using Eq. (2.6) we obtain the spectra

$$I_{x,y}(\omega)=\sum_{m_1,m_2}^{\infty} C_{x,y}(m_1,m_2)\,\delta^2(\omega-m_1\Omega-m_2\omega_L), \tag{4.6a}$$

$$I_z(\omega)=\frac{E_0^2}{4c^3(\Omega^2-\omega_L^2)^2}[2\Omega^4\delta^2(\omega-\Omega) + \omega_L^2(\Omega^2+\omega_L^2)\,\delta^2(\omega-\omega_L)], \tag{4.6b}$$

where the amplitudes for the positive x and y observation directions are given by

$$C_x(m_1,m_2)\equiv\frac{\Omega^2E_0^2\omega^2}{c^3(\Omega^2-\omega_L^2)^2}\left\{J'_{m_1}\left(\frac{E_0\omega}{c(\Omega^2-\omega_L^2)}\right)\times J_{m_2}\left(\frac{E_0\omega}{c(\Omega^2-\omega_L^2)}\right) + J'_{m_2}\left(\frac{E_0\omega}{c(\Omega^2-\omega_L^2)}\right)J_{m_1}\left(\frac{E_0\omega}{c(\Omega^2-\omega_L^2)}\right)\right\}^2, \tag{4.6c}$$

$$C_y(m_1,m_2)\equiv\frac{E_0^2\omega^2}{c^3(\Omega^2-\omega_L^2)^2}\left\{\Omega J'_{m_1}\left(\frac{E_0\omega}{c(\Omega^2-\omega_L^2)}\right)\times J_{m_2}\left(\frac{\Omega E_0\omega}{c\omega_L(\Omega^2-\omega_L^2)}\right) + \omega_L J'_{m_2}\left(\frac{\Omega E_0\omega}{c\omega_L(\Omega^2-\omega_L^2)}\right)\times J_{m_1}\left(\frac{E_0\omega}{c(\Omega^2-\omega_L^2)}\right)\right\}^2, \tag{4.6d}$$

where the arguments $E_0\omega/c(\Omega^2-\omega_L^2)$ and $\Omega E_0\omega/[c\omega_L(\Omega^2-\omega_L^2)]$ are just the ratio of the maximum displacement in the x and y directions to the wavelength of the scattered light frequency. The model equations of motion Eq. (4.5) neglected any kinematic relativistic effects and also the magnetic-field component of the laser, so the presence of the higher harmonics in Eq. (4.6) is exclusively a relativistic effect due to retardation. In view of the fact that there are no fitting parameters in the simple theory, the agreement between the model predictions for the peak positions and heights and the numerical data in Fig. 4 is good.

C. Resonant electric- and magnetic-field regime

In contrast to the case discussed in Sec. III, we are not aware of any nonperturbative analytical solution to a laser driven relativistic electron in a magnetic field and unfortunately one has to rely mainly on numerical results. In order to understand systematically how the scattered light spectra are modified by the magnetic field for relativistic laser fields, we have monitored first the time-dependent position of the electrons during the interaction with the laser pulse and recorded the maximum value of the elongation along the x direction, $x_{\max}$. The same simulation was then repeated for various magnetic-field strengths Ω to compute the function $x_{\max}(\Omega)$. In the nonrelativistic regime (corresponding to $E_0<0.1$ a.u.), the maximum elongation matches the prediction according to purely nonrelativistic response with a single resonance, $x_{\max}=E_0/|\Omega^2-\omega_L^2|$, associated with Eq. (4.5). In Fig. 5 we show the maximum elongations as a function of

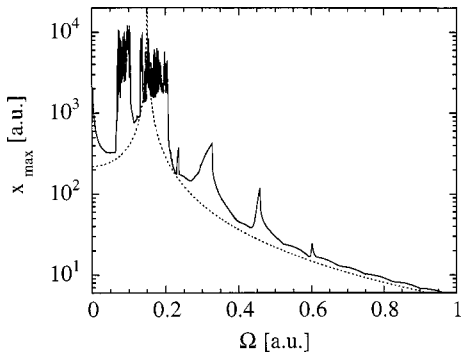

FIG. 5. Relativistic resonances due to the magnetic field. The maximum electron displacement $x_{\max}$ during the laser pulse as a function of the magnetic-field strength Ω. The dashed line is $x_{\max}=E_0/|\Omega^2-\omega_L^2|$ corresponding to the amplitude associated with a simple nonrelativistic model. The pulse was linearly turned on and off over two cycles and had a total duration of 34 cycles with a maximum amplitude $E_0=5$ a.u.

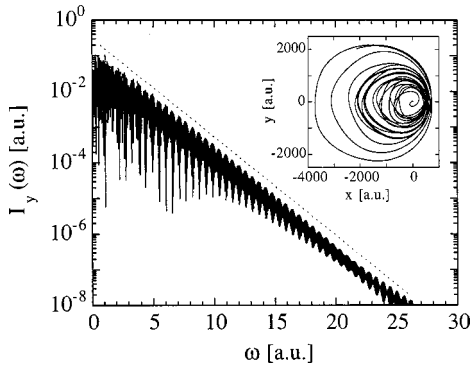

FIG. 6. The spectrum $I_y(\omega)$ at the cyclotron resonance. Scattered light spectrum in the laser field with frequency $\omega_L=0.15$ a.u., $E_0=5$ a.u., and $\Omega=\omega_L$. To illustrate the exponential fall-off, we have added a straight dashed line. The inset shows the corresponding orbit in the (x,y) plane. The nucleus is located at (0,0).

the magnetic field Ω recorded for a trapezoidal pulse with $E_0=5$ a.u. and a duration of 34 cycles with a two-cycle turn-on and turn-off. The graph does not change too much if the pulse duration is doubled to 68 cycles, which suggests that the interaction time was long enough for most resonances to develop. The dashed line corresponds to the amplitude $E_0/|\Omega^2-\omega_L^2|$, which allows only for a single (cyclotron) resonance at $\Omega=\omega_L$. The mismatch for $\Omega=0$ is expected since the (relativistic) drift along the y direction (which is rotated into the x direction by the magnetic field) cannot be predicted by the simple model described above.

The graph in Fig. 5 shows (at least) two windows $\Omega\in[0.06,0.10]$ and $\Omega\in[0.13,0.21]$ for which the maximum elongation depends in an erratic fashion on the B field. Small changes in the magnetic field modify the corresponding orbits drastically. Note that these irregular windows are located around $\Omega=\omega_L/2$ and the cyclotron resonance $\Omega=\omega_L$. The size of these two windows depends on the laser amplitude E_0. For $E_0<1$ a.u., we find only monotonic increases and decreases of $x_{\max}$ around the resonances, but for $E_0=20$ a.u., e.g., this irregular belt covers a much larger range in magnetic-field strength: $\Omega\in[0.03,0.64]$. The irregular nature of the orbits close to the resonances is also reflected in the scattered light spectra, some of which do not show nicely resolved higher harmonics. This regime is, of course, highly nonlinear due to the combination of the effects by the laser field, the magnetic-field component of the laser, and the cyclotron resonance.

The numerical spectra at the resonance $\Omega=\omega_L$ suggest that for large frequencies the intensity falls off exponentially, where the fall-off rate increases with decreasing laser field strength E_0. A sample spectrum is shown in Fig. 6; for comparison we have added a straight line to illustrate the exponential behavior. An exponential fall-off behavior is also characteristic of the spectrum of the much simpler case of a closed circular orbit which has been studied in detail to explain the radiation in synchrocyclotrons [38–40]. Circular orbits contain only a single fundamental rotation frequency and the higher harmonics in the synchrocyclotron spectrum are exclusively due to relativistic retardation effects. In our case, however, the orbit itself already contains a wide variety of frequencies. The inset of Fig. 6 shows the corresponding trajectory. The orbit is not closed and, depending on the parameter E_0, can perform a variety of quasicircular orbits with time-varying instantaneous radii and quasiperiodic modulations superimposed on the path. After the laser pulse is turned off, the orbits settle in a single circular orbit, whose center is shifted from the location of the nucleus. The corresponding after-pulse radius can be larger or smaller than the spatial extent during the pulse depending on the details of the laser pulse shape and also depending on its amplitude. The dependence of the velocity as a function of time (not shown) also illustrates the irregular character of the orbits at resonance. The graph contains several abrupt changes on a small time scale, which then can lead to large frequency components in the spectrum. Along the z direction, however, the spectra contain almost no high-frequency components, which is consistent with the fact that a relativistic particle radiates mainly into a small cone in the forward direction of its motion in the x-y plane.

Let us now return to the other resonances manifest in Fig. 5. The resonances associated with multiples of the laser frequency $\Omega=n\omega_L$ are apparent, where $n=2,3,4$ and even a very narrow resonance close to $\Omega=3\omega_L/2$ is visible. It is quite interesting to note the unusual, sawtooth shape of the resonances. This surprising shape seems to be inherent to those resonances that are associated with an integer multiple of the laser frequency $\Omega=n\omega_L$. Quite curiously, the expected resonance location $\Omega=n\omega_L$ does not agree with the local maximum value of each ''sawtooth.'' In each case the numerical value $\Omega=n\omega_L$ agrees much better with the location of the geometrical center of each sawtooth. To illustrate this point, we have enlarged the peak around the cyclotron resonance $\Omega=\omega_L$ on a linear scale for $E_0=1$ a.u. in Fig. 7(a). In this case the main peak is also accompanied by a symmetric resonance around $\Omega=\omega_L/2$, which demonstrates that, at least in principle, resonances can occur if ω_L and Ω are commensurate. The sharp decrease at $\Omega=0.1726$ a.u. ($x_{\max}=1100$ a.u.) to $\Omega=0.1730$ a.u. ($x_{\max}=417$ a.u.) is remarkable.

In Fig. 7(b) we show the time dependence of the coordinate $x(t)$ of the two trajectories associated with these two nearby parameters Ω. The dashed line is associated with the orbit for the smaller B field ($\Omega=0.1726$ a.u.). The two orbits

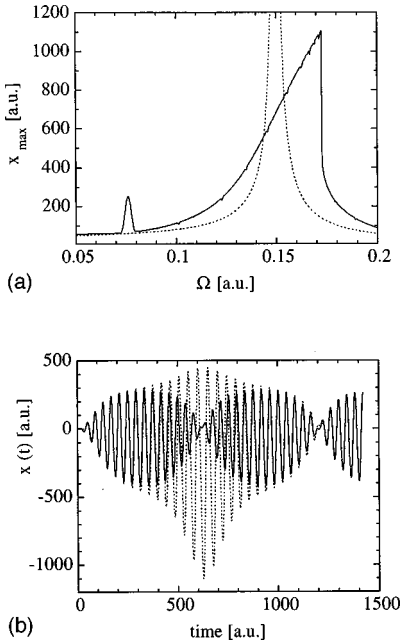

FIG. 7. The cyclotron resonance profile. (a) The maximum electron displacement $x_{\max}$ during each laser pulse as a function of the magnetic-field strengths Ω. The dashed line is $x_{\max}=E_0/|\Omega^2-\omega_L^2|$ corresponding to the amplitude associated with a simple nonrelativistic model. The pulse was linearly turned on and off over two cycles and had a total duration of 34 cycles with a maximum amplitude $E_0=1$ a.u. (b) Two orbits responsible for the steep decrease in (a). The orbit displayed by the straight (dashed) line corresponds to $\Omega=0.1726$ a.u. ($\Omega=0.1730$ a.u.).

are practically identical during the first seven optical cycles of the pulse, but then one orbit shrinks whereas the other one grows. After about 22 optical cycles, both orbits become very similar again. Both orbits oscillate approximately on the time scale of the optical period. The maximum velocity in the x and y direction is around 55 a.u. for one trajectory, whereas the other trajectory has a maximum velocity of 95 a.u. in each coordinate direction. It is obvious that these two qualitatively different types of orbits will also lead to different scattered light spectra. The motion along the y direction (not shown) is very similar to that of the x direction.

In Fig. 8 we demonstrate how the scattered light spectra change due to the relativistic resonances around $\Omega=2\omega_L$ and $\Omega=3\omega_L$. In Fig. 8(a) we have examined the spectra $I_x(\omega)$ in the close vicinity of $\Omega=2\omega_L$ corresponding to $\Omega=0.28$, 0.30, and 0.32 a.u. The off-resonant spectra (a) and (c) are very similar. The main peaks can be associated with multiples of the laser frequency ω_L, and the small narrow peaks that accompany the peaks on the left- [in (a)] and right-hand side [in (c)] are the integer multiples of Ω. The spectrum associated with the resonance (b) shows that the harmonics of the laser and also those of the magnetic field can become significantly increased. With the exception of the laser fundamental frequency, practically each peak is increased by several orders in magnitude. We found that in general those laser multiples whose frequency ω is smaller than the resonant value of Ω were typically only slightly affected by the resonance. This becomes obvious if we analyze the three-photon resonance in Fig. 8(b). The two peaks for which $\omega<\Omega$ are not so much changed by the resonance.

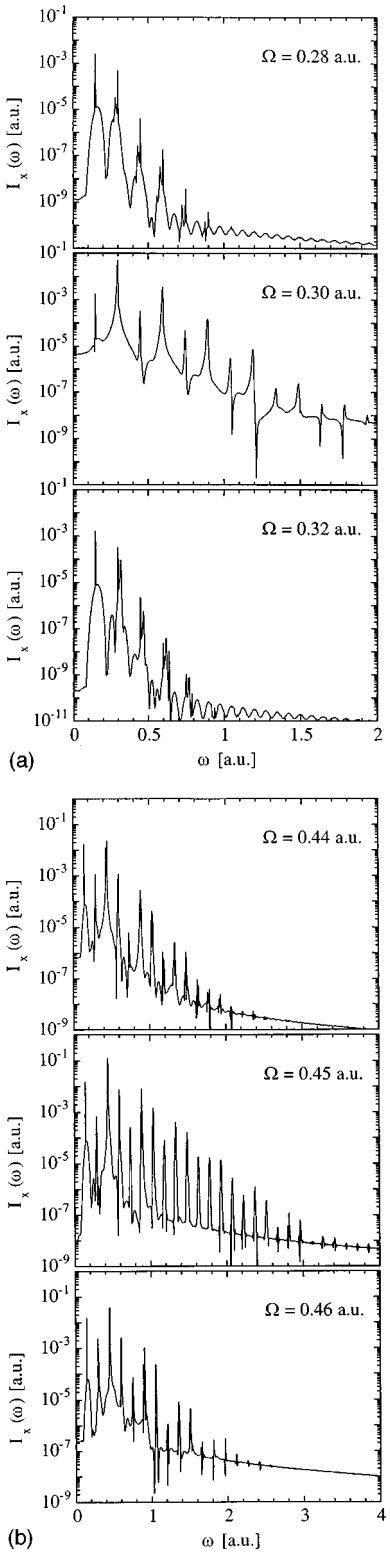

FIG. 8. Enhancement of harmonics due to relativistic resonances. Scattered light spectrum $I_x(\omega)$ for $\omega_L=0.15$ a.u. and three values of the magnetic field Ω. (a) Around the two-photon resonance $\Omega=2\omega_L=0.30$ a.u., $E_0=1$ a.u. (b) Around the three-photon resonance $\Omega=3\omega_L=0.45$ a.u., $E_0=5$ a.u.

Again, the even- and odd-order harmonics at the resonance $\Omega=3\omega_L$ are drastically enhanced.

In all of the spectra we have noted that the redshifts present in the magnetic-field-free spectra discussed in Sec.

III do not occur since the curved orbits prohibit the irreversible drift due to the magnetic-field component of the laser. To the contrary, the effective Doppler shift that one could calculate from a time-averaged shift computed over a circular orbit in the *x-y* plane is actually shifted to a higher effective frequency.

V. DISCUSSION

It is obvious that the present work will raise more questions than it can answer. The relativistic interaction of laser-driven electrons in extremely strong static homogeneous magnetic fields is a relatively unexplored area. The strength of the *B* field discussed in this work is certainly smaller than that of neutron stars, but on the other hand they are several orders of magnitude larger than the static fields generated by nondestructive magnets in a laboratory setup in the millisecond range [41]. Very recently, Kudasov *et al.* [42] have produced static magnetic-field bursts of μs duration and a maximum amplitude of 1000 T.

Past work for the more simple case of the circular synchrocyclotron motion showed good coincidence with the theory of radiation of a single classical electron [36]. However, preliminary simulations using return maps for large laser intensities [43] have indicated the emergence of possible chaotic behavior due to the nonlinear relation between momentum and velocity. The departure between quantum and classical predictions is well known to be enhanced for systems exhibiting chaotic motion [44]. Therefore, possible modifications in the scattered radiation spectrum due to the quantum-mechanical nature of the electron are possible for our system. Extensions for the spectra could be computed from time-dependent solutions to the full Dirac equation [45]. A work in this direction is presently underway and will be reported elsewhere. The nonrelativistic synchrotron motion of electrons in a circle is fully coherent, but the radiation by relativistic orbits at least in the region of high frequencies requires incoherent corrections. A similar question must be addressed for the relativistic resonances as well.

In the relativistic regime the effects due to the back reaction of the generated fields on the electron's orbit could become relevant. A recent work by Keitel *et al.* [46] has solved the classical Lorentz-Dirac equation to investigate the radiative reaction for strong-field ionization and concluded that this effect is relatively small even for intensities of the order of 10^{20} W/cm^2 and visible frequencies.

The single-trajectory spectra were investigated as a first step to better understand the spectra for an ensemble of electrons. It is obvious that the ensemble-averaged spectra cannot contain frequencies that are not manifest in the single-trajectory spectrum. At least in the weak-field case, only the latter should be compared directly with the predictions of a full quantum calculation. Most of our preliminary calculations that included averaging over a classical ensemble basically confirmed what one might expect. The ensemble averages enhance spectral properties that are independent of the individual trajectories' initial condition and spectral features that are induced by the external field add up coherently, as most of the electron orbits follow the field in a similar fashion. Those spectral components that depend on the initial condition of the orbit are averaged out.

Our original motivation to introduce an additional strong magnetic field to the dynamics was to increase the dynamical impact of the atom's nonlinearity by confining the electron's motion closer to the nucleus. In contrast to the ''traditional'' higher harmonics in the nonrelativistic regime that have been directly associated with this nonlinearity as discussed in the rescattering model, the main features of the spectra in the relativistic case seem to be dominated by the dynamical impact of the nonlinearities associated with the relativistic coupling to the external laser and magnetic fields. We discovered that relativistic resonances, which have not been discussed before, can be exploited to increase the production of higher harmonics significantly [47]. With the exception of the cyclotron frequency $\Omega = \omega_L$, these resonances have no nonrelativistic counterpart in the dipole approximation.

ACKNOWLEDGMENTS

We acknowledge helpful conversations with D. L. Holland and R. F. Martin. This work has been supported by the NSF under Grant No. PHY-9970490. We also acknowledge support from the Research Corporation and ISU for URGs. R.E.W. thanks the Illinois State University Undergraduate Honors Program for support of his research work. The animated graphics of the spectra on the web site http://www.phy.ilstu.edu/ILP were generated by P. J. Peverly and T. R. Shepherd.

[1] For review articles and monographs on high-order harmonic generation, see *Multiphoton Processes*, edited by G. Mainfray and P. Agostini (CEA, Paris, 1991); *Atoms in Intense Laser Fields*, edited by M. Gavrila (Academic, Boston, 1992); *Multiphoton Processes*, edited by D. K. Evans and S. L. Chin (World Scientific, Singapore, 1994); *Super-Intense Laser-Atom Physics*, edited by B. Piraux, A. L'Huillier, and K. Rzazewski, Vol. 316 of *NATO Advanced Study Institute Series B: Physics* (Plenum, New York, 1993); L. F. DiMauro and P. Agostini, Adv. At., Mol., Opt. Phys. **35**, 79 (1995); *Super-Intense Laser-Atom Physics IV*, edited by H. G. Muller and M. V. Fedorov, Vol. 13 of *NATO Advanced Study Institute Series 3: High Technology* (Kluwer Academic, Dordrecht, 1996).

[2] J. Zhou, J. Peatross, M. M. Murnane, H. C. Kapteyn, and I. P. Christov, Phys. Rev. Lett. **76**, 752 (1996).

[3] C. Spielmann, N. H. Burnett, S. Sartania, R. Koppitsch, M. Schnürer, C. Kan, M. Lenzner, P. Wobrauschek, and F. Krausz, Science **278**, 661 (1997).

[4] Z. Chang, A. Rundquist, H. Wang, M. M. Murnane, and H. C. Kapteyn, Phys. Rev. Lett. **79**, 2967 (1997).

[5] Y. Kobayashi, T. Sekikawa, Y. Nabekawa, and S. Watanabe, Opt. Lett. **23**, 64 (1998).

[6] K. C. Kulander, K. J. Schafer and J. L. Krause, in *Super-Intense Laser-Atom Physics*, edited by B. Piraux, A. L'Huillier and K. Rzazewski, Vol. 316 of *NATO Advanced Study Institute Series B: Physics* (Plenum, New York, 1993), p. 95.

[7] P. B. Corkum, Phys. Rev. Lett. **71**, 1994 (1993).
[8] P. Dietrich, N. H. Burnett, M. Ivanov, and P. B. Corkum, Phys. Rev. A **50**, R3585 (1994).
[9] For a review, see *Atoms in Intense Laser Fields* (Ref. [1]).
[10] P. Salieres, A. L'Huillier, and M. Lewenstein, Phys. Rev. Lett. **74**, 3776 (1995).
[11] C. Kan, N. H. Burnett, C. E. Capjack, and R. Rankin, Phys. Rev. Lett. **79**, 2971 (1997).
[12] M. B. Gaarde, P. Antoine, A. L'Huillier, K. J. Schafer, and K. C. Kulander, Phys. Rev. A **57**, 4553 (1998).
[13] F. I. Gauthey, C. H. Keitel, P. L. Knight, and A. Maquet, Phys. Rev. A **55**, 615 (1997).
[14] For a recent work on the phase dependence of the HHG, see, e.g., A. de Bohan, P. Antoine, D. B. Milosevic, and B. Piraux, Phys. Rev. Lett. **81**, 1837 (1998).
[15] P. Salieres, P. Antoine, A. de Bohan, and M. Lewenstein, Phys. Rev. Lett. **81**, 5544 (1998).
[16] M. Lewenstein, P. Salieres, and A. L'Huillier, Phys. Rev. A **52**, 4747 (1995).
[17] C. H. Keitel, P. L. Knight, and K. Burnett, Europhys. Lett. **24**, 539 (1993); C. H. Keitel and P. L. Knight, Phys. Rev. A **51**, 1420 (1995).
[18] J. P. Connerade and C. H. Keitel, Phys. Rev. A **53**, 2748 (1996).
[19] T. Zuo, A. D. Bandrauk, M. Ivanov, and P. B. Corkum, Phys. Rev. A **51**, 3991 (1995).
[20] D. B. Milosevic and A. F. Starace, Phys. Rev. Lett. **82**, 2653 (1999).
[21] M. Gajda, J. Grochmalicki, M. Lewenstein, and K. Rzazewski, Phys. Rev. A **46**, 1638 (1992).
[22] J. D. Jackson, *Classical Electrodynamics* (Wiley, New York, 1975).
[23] The spectral manifestation of periodic Kepler orbits was investigated by G. Bandarage, A. Maquet, and J. Cooper, Phys. Rev. A **41**, 1744 (1990).
[24] G. Badarage, A. Maquet, T. Menis, R. Taieb, and V. Veniard, Phys. Rev. A **46**, 380 (1992).
[25] L. Landau and L. Lifshitz, *The Classical Theory of Fields*, 2nd ed. (Pergamon, London, 1990). For an explicit solution, see J. Krüger and M. Bouyn, J. Phys. A. **9**, 1841 (1976).
[26] N. D. Sengupta, Bull. Math. Soc. (Calcutta) **41**, 187 (1949); **41**, 189 (1949).
[27] J. H. Eberly and A. Sleeper, Phys. Rev. **176**, 1570 (1968).
[28] For an experimental signature of this motion, see Phys. Today **52** (2), 9 (1999); S. Y. Chen, A. Maksimchuk, and D. Umstadter, Nature (London) **396**, 653 (1998).
[29] J. H. Eberly, in *Progress in Optics 7*, edited by E. Wolf (North-Holland, Amsterdam, 1969).
[30] E. S. Sarachik and G. T. Schappert, Phys. Rev. D **1**, 2738 (1970).
[31] Y. I. Salamin and F. H. M. Faisal, Phys. Rev. A **54**, 4383 (1996).
[32] For computer movies of these spectra, see http://www.phy.ilstu.edu/ILP/hhgrefs.html
[33] The homogeneous solution has been discussed in Landau and Lifshitz [25].
[34] For a collection of the few analytically soluble cases, see V. G. Bagrov and D. M. Gitman, *Exact Solutions of Relativistic Wave Equations* (Kluwer Academic, Dordrecht, 1990).
[35] G. A. Schott, *Electromagnetic Radiation* (Cambridge University Press, Cambridge, 1912).
[36] For a review, see R. P. Godwin, in *Springer Tracts in Modern Physics Vol. 51*, edited by G. Höhler (Springer-Verlag, Berlin, 1969), pp. 1–73; A. A. Sokolov and I. M. Ternov, *Synchrotron Radiation* (Akademie-Verlag, Berlin, 1968).
[37] J. Schwinger, Phys. Rev. **75**, 1912 (1945).
[38] F. R. Elder, R. V. Langmuir, and H. C. Pollock, Phys. Rev. **74**, 52 (1948).
[39] D. H. Tomboulain and P. L. Hartman, Phys. Rev. **102**, 1423 (1956).
[40] G. Bathow, E. Freytag, and R. Hänsel, J. Appl. Phys. **37**, 3449 (1966).
[41] For a review on recent developments of nondestructive 100-T magnets, see Phys. Today **51** (10), 21 (1998).
[42] Yu. B. Kudasov *et al.*, Pis'ma Zh. Eksp. Teor. Fiz. **68**, 326 (1998) [JETP Lett. **68**, 350 (1998)].
[43] R. F. Martin, R. E. Wagner, Q. Su, and R. Grobe (unpublished).
[44] F. Haake, *Quantum Signatures of Classical Chaos* (Springer, Berlin, 1991).
[45] J. W. Braun, Q. Su, and R. Grobe, Phys. Rev. A **59**, 604 (1999).
[46] C. H. Keitel, C. Szymanowski, P. L. Knight, and A. Maquet, J. Phys. B **31**, L75 (1998).
[47] R. E. Wagner, Q. Su, and R. Grobe, Bull. Am. Phys. Soc. **44**, No. 1, 634 (1999).